

# Behaviour of corroded steel angle compression members – numerical study

Katalin Oszvald / László Dunai

Received 2012-10-24, accepted 2013-01-03

## Abstract

*The paper is on the behaviour of corroded angle section members under centric compression. The structural elements, with different cross-sections and slenderness, are studied by finite element analysis. The joint effects of various corrosion parameters are studied. The behaviour modes are determined in the function of the parameters of the corrosion and the cross-section characteristics. Conclusions are drawn on the decreasing tendency of the ultimate load.*

## Keywords

*corrosion · angle – section · compression member · stability · numerical analysis*

## 1 Introduction

### 1.1 General

Corrosion is one of the most common problems of steel structures. The different weather circumstances and the lack of the maintenance are leading to corrosion. The corrosion influences both the material properties and the surface conditions. In civil engineering practice the corrosion usually causes only surface changes; first the paint comes off in flakes and then the element thickness is reduced. The appearance and rate of the corrosion can be various therefore different parameters (e.g. thickness reduction, position and extension of corrosion) are to be defined to characterise the phenomenon. The knowledge of the behaviour and the resistance of the corroded elements are important to decide whether the elements must be replaced or it is enough to strengthen it. The recent codes of steel structures (Eurocode [1], CAN/CSA, AISC, ASCE) give only minor recommendation [2], how to consider the effect of corrosion in the analyses of the elements. Typically the average cross-section is proposed by the standards, but in general this approximation is not accurate enough due to the diversity of the corrosion.

### 1.2 Literature overview

Several theoretical and experimental studies are completed on the effect of corrosion on the behaviour and the remaining capacity of steel elements. Rahgozar analysed corroded I-section beams [3] and determined minimum curves to estimate the remaining capacity of the members in the function of the loss of thickness and the failure types. In the study the assumed corrosion type was uniform corrosion along the whole member. The rate of the web and flange thickness reduction was various in the analyses. Experimental and analytical analyses were carried out and the different failure modes (shear, lateral torsional buckling, bearing failure) were determined. The study showed that different rate of thickness reduction lead to various failure modes and the plate slenderness of the cross-section is changed by the corrosion. Peak et al. investigated sheared steel plate elements with pitting corrosion [4, 5]. Parametric nonlinear finite element analyses were carried out and closed-form design formula was proposed to calculate the ultimate strength of the

## Katalin Oszvald

Department of Structural Engineering, Budapest University of Technology and Economics, H-1111 Budapest, Műegyetem rkp. 3., Hungary  
e-mail: oszvaldkata@gmail.com

## László Dunai

Department of Structural Engineering, Budapest University of Technology and Economics, H-1111 Budapest, Műegyetem rkp. 3., Hungary

pitted plates. Jiang and Soares investigated pitted steel plates under biaxial compression [6]. Khedmati et al. analysed corroded plates with both-sided randomly distributed pits under uniaxial compression [7]. The effect of localized corrosion on plate buckling was investigated by Sadovsky and Dradcky [8]. Nakai et al. carried out extensive analyses on hold frames of bulk carriers [9, 10]. The research involved tensile tests, buckling tests, 3- and 4-point-bending tests and finite element analyses on pitting corroded elements. Angle section members – in the subject of the current study – were previously analysed by Beaulieu et al. [2]. The specimens were corroded artificially by galvanic process and the tests results were compared to the analytical results calculated according to the proposals of the relevant Canadian and American standards. In the test set-up eccentric compression was applied by gusset plate. Comprehensive study on corroded steel angle compression members, analyzing the effect of the main corrosion parameters has not been found in the literature. Extended studies were, however, completed on non-corroded compression angle members; Liu et al. analysed equal and unequal single steel angle elements by tests and numerical methods [11–13]. The effect of the eccentricity, the behaviour and the ultimate load were determined on equal section element and the test results were compared to the resistances obtained from standards and other suggested process. The observed failure modes were flexural and flexural-torsional buckling, depending on the eccentricity.

### 1.3 Purpose and scope

The aim of the current research is to discover the stability behaviour of corroded compression angle members by a comprehensive numerical study. In the study it is aimed to consider the diversity of the corrosion applying different corrosion patterns, thickness reductions, extension and position of the corrosion. The relevant behaviour modes and the resistance decreases are to be determined in the function of the introduced corrosion parameters.

## 2 Experimental background

In the first phase of the research experimental study is carried out on twenty-four specimens by the authors [14]. In the tests centric compression is applied and the effects of the following damages are analysed: uniform, pitting and local corrosion. The corrosion is modelled by thickness reduction, the thickness of the legs is reduced by artificial mechanical process. The dimension of the cross-section is 40×40×4 mm, the nominal length of the member is 790 mm and the effective length (distance between the bearing ball supports) is 840 mm. Hinge support is applied in the cross-sectional centroid of the non-corroded members. The buckling behaviour and the relationship between the corrosion reduction and the resistance decrease are determined.

The observed typical failure modes are shown in Fig. 1. The governing buckling mode is flexural buckling for uniform and pitting corrosion specimens, and local plate buckling for locally

corroded specimens in the investigated cases. The rate of the cross-section reduction is various in terms of the corrosion types and the other corrosion parameters. The results showed that the prediction of the resistance on the basis of the maximal cross-section reduction results in better approach comparing to the average cross-section reduction based calculation. The maximal cross-section reduction is calculated as the maximal cross-section decrease in the member compare to the gross area, and the average cross-section reduction as the ratio of the corroded volume comparing to the total original volume of the specimen. The resistances are compared to the Eurocode based calculations; it is concluded that the standard buckling resistances can be used as conservative estimation by applying the maximal cross-section reduction. The experiments are used as validation background of the finite element model development.

## 3 Finite element modelling

### 3.1 Corrosion modelling

The stability behaviour of the corroded compression angle is simulated by finite element model. The corrosion is modelled by thickness reduction similarly to the previous numerical studies [5–7]. In the ANSYS [15] finite element software environment a 4-node shell element (SHELL 181) is applied, which can model thin and moderately thick plated structures and it is well-suited for large strain nonlinear applications. Note that this finite element was applied in Liu's numerical study [12] of non-corroded angle elements under compression and by Kövesdi et al. [16] to investigate stability problems of steel girders with trapezoidal webs. In case of shell models the different continuously rough surface cannot be modelled accurately if the corrosion is different on the two sides of the legs. In order to consider the corroded geometry more accurately, solid model is used, by applying 20-node-element (SOLID186). The element supports elastic-plastic material behaviour, large deflection, and large strain capabilities.

To facilitate the numerical analyses, a parametric code is programmed in ANSYS own language (APDL). In the algorithm the location, the extent and the distribution parameters of the corrosion are considered. In the algorithm of the pitting corrosion the distribution of the pitting can be completed randomly or uniformly, using solid elements. Similar algorithm is developed and programmed for uniform corrosion using shell elements. Figure 2 illustrates the different corrosion models.

The steel is modelled as linear elastic – perfectly plastic material; steel grade S235 is used, with the nominal yield strength of  $f_y = 235 \text{ N/mm}^2$ ; the Young's modulus is  $210000 \text{ N/mm}^2$  and the Poisson's ratio is 0.3.

The support condition is hinge connection, the same as in the compressive buckling tests.

### 3.2 Model calibration and validation

#### 3.2.1 Centric compressive buckling tests

The developed shell and solid models are calibrated in the preliminary study on the bases of the executed tests. The geom-

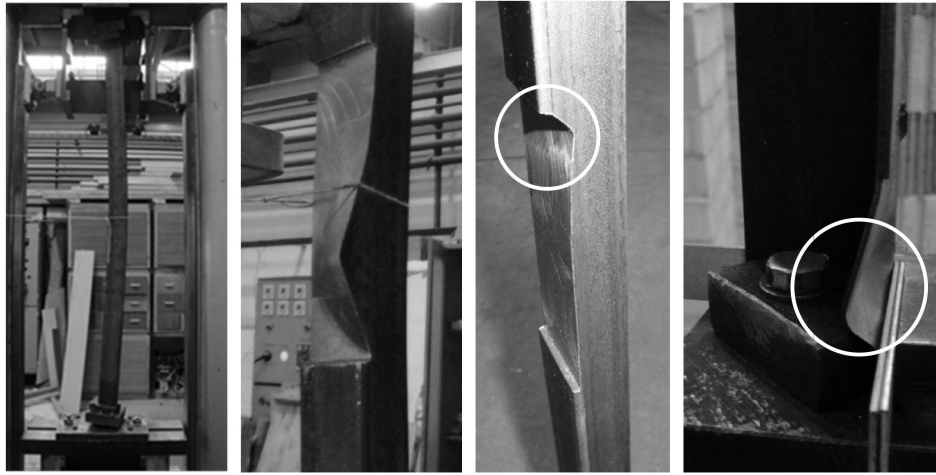


Fig. 1. Behaviour modes of centric compressed members

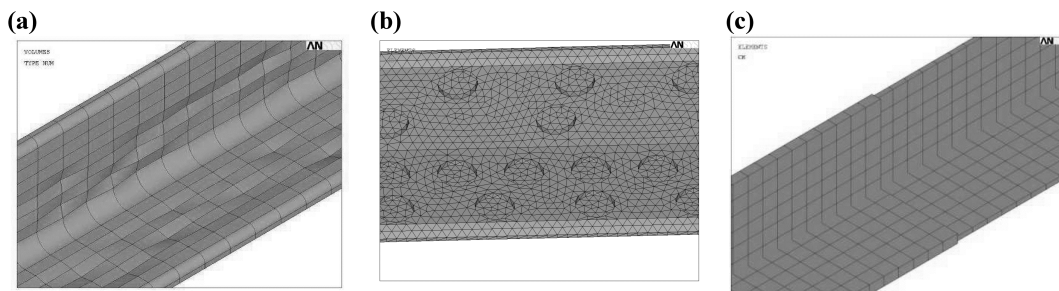


Fig. 2. Numerical models: (a) solid model for thickness reduction; (b) solid model for pitting corrosion; (c) shell model for thickness reduction

etry of the corroded specimens are modelled and the measured yield stresses are used in the geometrically and material nonlinear imperfect analyses (GMNI). The shape of first buckling mode of the stability analysis is applied as initial geometric imperfection. Its magnitude is calibrated on the basis of the measured resistances. Both solid and shell models are applied in the analyses. The accuracy and the efficiency of the models are evaluated on the basis of element types and sizes [17].

Fifteen investigated members of the preliminary study are illustrated in Table 1. On schematic figure of the specimens both legs are illustrated and the black colour marks the corrosion. The position of the corrosion is detailed on the figures. The cross-section reduction of the members is given in  $M_{corr}$  column. Table 1 contains  $N_{b,m}$ , the measured maximal load of the test and the ultimate load of the numerical models:  $N_{b,SHELL}$  and  $N_{b,SOLID}$ . In the notation the subscript marks the finite element types applied in the numerical analyses. The ratios of the numerical analysis and the test results are also presented in Table 1. In the case of the shell model the applied magnitude of geometrical imperfection is between  $L/400 - L/2000$  and for solid model it is between  $L/100 - L/1500$ , where  $L$  is the length of the compression member.

The results of the preliminary study are illustrated by the load-displacement curves of specimen L4 in Fig. 3(a). Figure 3(b) shows the local buckling failure mode of specimen L3. In Fig. 3(a) the results show that both shell and solid models are in good agreement with the test.

### 3.2.2 Eccentric loading tests

The numerical model is verified under eccentric loading conditions, too, on the basis of the tests of Liu et al. [11]. In the nonlinear analyses the geometrical and the material properties of the investigated elements are the same as in tests, as detailed in [11]. The measured average initial geometric imperfection ( $L/2100$ ) is used in the analyses. Table 2 contains the same ID of the elements as in [11] and the same measured eccentricities. In the table the measured ultimate load of the tests  $R_M$ , the results of the numerical analyses are detailed. The ratio of the numerical and the test results and the mean value and the coefficient of variation of the comparative ratios are also presented. The ultimate behaviour modes obtained by the FEM analyses correspond to the test results, the observed behaviours were flexural buckling and flexural-torsional buckling.

### 3.2.3 Evaluation of the model validation results

The results show that both shell and solid models can model the behaviour of the centric compressive corroded members. The disadvantage of the solid model is the small finite element size in (i) large number of model DOF's in the model and (ii) time consuming analysis. The results of the test can be more accurately estimated by solid finite element model, but the shell model also gives acceptable results.

In the eccentric tests it is observed that the shell model better approximates the test results: the mean value of the comparative ratio is 1.0, while this value is 1.06 in the case of solid model The

**Tab. 1.** Results of preliminary numerical study on centric compression members

ID	Location of corrosion	$M_{corr}$ [%]	$N_{b,m}$ [kN]	$N_{b,SHELL}$ [kN]	$N_{b,SHELL} / N_{b,m}$	$N_{b,SOLID}$ [kN]	$N_{b,SOLID} / N_{b,m}$
O2 (II)	—	0.0	50.33	48.73	0.97	50.75	1.01
A1 (I)		29.0	33.2	32.44	0.98	32.54	0.98
A4 (I)		14.7	50.95	43.60	0.85	50.86	1.00
A5 (I)		12.7	35.5	34.4	0.97	33.10	0.93
A6 (I)		18.8	33.6	33.6	1.00	33.03	0.98
A7 (I)		25	43.8	42.81	0.98	43.79	1.00
A8 (I)		25	37.7	37.03	0.98	37.14	0.98
A9 (II)		13	43.68	42.16	0.97	42.44	0.97
A10 (II)		13	38.5	38.6	1.00	38.58	1.00
A11 (II)		13	36.93	37.04	1.02	36.88	1.00
L1 (II)		70	14	12.88	0.92	14.15	1.01
L2 (II)		73.5	9.6	9.15	0.95	9.8	1.02
L3 (II)		76	4.9	4.99	1.02	4.65	0.95
L4 (II)		49.8	28.3	27.9	0.98	28.15	0.99
L5 (II)		27.8	34	33.98	1.00	34.19	1.00
				Mean value	0.97	0.98	
				C.O.V	4.1	2.3	

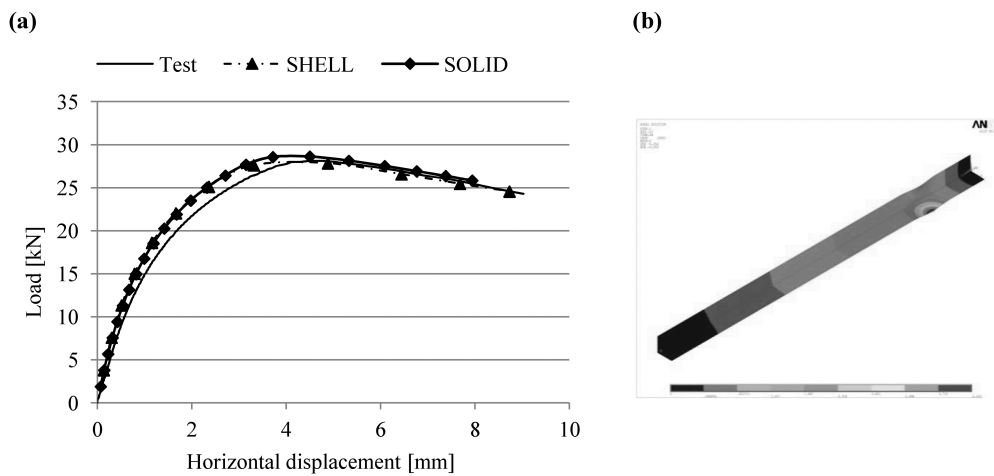


**Fig. 3.** Results of preliminary study: (a) load-displacement curves of specimen L4; (b) local buckling failure mode of specimen L3

C.O.V is also less in the case of shell model. It can be concluded that the shell model gives an acceptable approach to estimate the resistance of the eccentrically compressed angle specimen and it follows the observed behaviour. Having these findings in the further analysis the shell model is applied

#### 4 Numerical study program

In the frame of the numerical study program virtual experiments are completed. Bifurcation stability analysis (geometric non-linear buckling analysis – GNB) and geometrically and material non-linear imperfect analyses (GMNI) are completed on various corroded elements. The results of the GNB analysis provide with the shape of the initial geometrical imperfection for the nonlinear analyses; the magnitude is assumed at the level of  $L/200$ . In the GMNI analyses the ultimate behaviour and load are determined. Various size and patterns of corrosion are assumed, as detailed in the followings. Eleven basic elements are investigated with relative slenderness between 0.7-1.5, as shown in Table 3. The initial  $b/t$  (width-to-thickness) ratio is detailed, as the basis of the cross-section classification of angle-section elements by Eurocode 3. In the further evaluation of the corroded elements the  $b/t$  is the ratio of the reduced thickness and the width of the legs, as a corrosion parameter.

Two typical corrosion patterns are applied in the numerical study: in the case of pattern “A” the corrosion occurs on one leg and in case of pattern “B” both of the legs are corroded. The corrosion is marked by black on the simplified figure of the patterns in Table 4. The parameters which describe the corrosion in the study are as follows: the thickness reduction ( $T_{red}$ ), the extension of corrosion ( $Ext$ ) and the position of the corrosion ( $p_c$ ). The  $Ext$  parameter is equal to the ratio of the length of the corroded area to the total length. The  $p_c$  parameter is defined as the ratio of the centroid of the corroded area to the half of the length.

In the further evaluation the  $b/t$  ratio is an important parameter of the comparison. The same  $T_{red}$  parameter does not equal to the same  $b/t$  elements RF-1, RF-6, RF-9 because of the initial  $b/t$  ratio is different. Therefore consecutive GMNI analyses are carried out on further corroded elements, where the  $T_{red}$  is modified to have equal  $b/t$  ratio.

#### 5 Buckling modes

The aim of the GNB analysis is to get the first relevant buckling mode of the perfect elements to be applied in the GMNI analysis as imperfection. Three different stability modes are observed in the analyses (Fig. 4): flexural buckling about the weak axis, local plate buckling and torsional buckling in the corroded part. In the case of pattern “A” the first and second modes and in the case of pattern “B” the first and third modes are observed. The length of the local buckling wave is approximately two times the free width of the outstanding plates if the corrosion is on one leg (pattern “A”). In case of pattern “B” the length of the buckling wave is the length of the corroded area

The aim is to determine the relationship between the corrosion parameters and the buckling modes. In the case of the corroded element’s  $b/t$  ratio “sufficient” and “necessary” values are defined as follows: if the  $b/t$  is greater than a sufficient value the buckling mode is local buckling or torsional buckling depending on the corrosion patterns. If this parameter is less than the sufficient value, but greater than a necessary value the behaviour is determined by the other corrosion parameters (position and extension of corrosion). The “necessary” and the “sufficient”  $b/t$  values are different in the cases of the two patterns. Considering the relative slenderness Table 5 summarizes the necessary and the sufficient  $b/t$  values.

In Table 6 the various buckling modes are presented in the function of the extension ( $Ext$ ) and the position of corrosion ( $p_c$ ), the  $b/t$  ratio and the relative slenderness ( $\bar{\lambda}$ ). If the  $b/t$  ratio is greater than the “necessary”, but less than the “sufficient”, the following observations can be done:

- The numbers of the local and torsional buckling cases are increased as  $b/t$  approaches the sufficient value in cases, pattern “A” or “B” (as shown in Table 6 Part 1). The results belong to elements with pattern “B” and 0.7 relative slenderness. In these cases the decisive parameters are the position and the extension of corrosion to determine the buckling mode.
- Corrosion next to the support changes the buckling mode from global to torsional buckling if the extension of corrosion is 20%. More than 20% extension of corrosion causes change of buckling mode, from global to local. The maximal value of the extension for local mode depends on the  $b/t$  ratio and on the relative slenderness.
- In case of pattern “B” the same buckling modes are observed (Table 6 Part 3) irrespectively of the initial  $b/t$  ratio of the non-corroded element, beside the same parameters as  $b/t$ ,  $Ext$  and  $p_c$ .
- In case of pattern “A” the previous statement is not valid; in these cases the same  $b/t$ ,  $Ext$  and  $p_c$  parameters do not result in the same buckling mode (Table 6 Part 2). The reason is that the same  $b/t$  ratio belongs to different  $T_{red}$ , because of the different initial  $b/t$  ratio of the non-corroded elements. Therefore  $T_{red}$  is the governing parameter beside the  $b/t$  to determine the buckling mode.

#### 6 Ultimate behaviour

##### 6.1 Behaviour modes

In the next phase of the numerical study GMNI simulations are carried out on the corroded elements. The observed behaviour modes are generally determined by the applied buckling shapes, as geometrical imperfections. Flexural buckling is observed in the case of global buckling mode about the weak axis. Yield mechanism developed in the half of the member on non-corroded member, but it shifted on the corroded members



**Tab. 2.** Results of preliminary numerical study on eccentric compression members

No.	Specimen ID	$e_x$ [mm]	$e_y$ [mm]	$R_M$ [kN]	$R_{SOLID}$ [kN]	$R_{SOLID}/R_M$	$R_{SHELL}$ [kN]	$R_{SHELL}/R_M$
1	E900-1	0	0	117	124.35	1.06	105.34	0.90
2	E900-2	4.2	0	110.9	118.68	1.07	107.29	0.97
3	E900-3	10	0	105.3	106.06	1.01	102.56	0.97
4	E900-4	16.8	0	84.5	80.71	0.96	99.48	1.18
5	E900-5	29.4	0	59	58.86	1.00	60.32	1.02
6	E900-6	50.4	0	46.1	41.55	0.90	40.42	0.88
7	E900-7	0	8.4	65.6	66.19	1.01	61.46	0.94
8	E900-8	0	16.8	46.4	49.65	1.07	46.09	0.99
9	E900-9	0	29.4	34.4	36.45	1.06	33.92	0.99
10	E900-10	0	50.4	23.3	25.6	1.10	23.65	1.02
11	E1200-1a	4.2	0	68.1	73.65	1.08	67.84	1.00
12	E1200-1b	4.2	0	69.7	73.65	1.08	67.84	0.97
13	E1200-2	10	0	66.7	73.56	1.10	66.27	0.99
14	E1200-3a	16.8	0	66.4	73.29	1.10	66.27	1.00
15	E1200-3b	16.8	0	71.3	72.36	1.01	65.03	0.91
16	E1200-4	29.4	0	57	53.36	0.94	57.17	1.00
17	E1200-5	50.4	0	42.5	39.47	0.93	40.73	0.96
18	E1500-1a	0	0	45.3	50.98	1.13	46.61	1.03
19	E1500-1b	0	0	41.1	50.98	1.13	46.61	1.13
20	E1500-1c	0	0	42.8	50.98	1.13	46.61	1.09
21	E1500-2	8.4	0	42.9	50.99	1.19	46.36	1.08
22	E1500-3	16.8	0	41.3	50.81	1.23	45.55	1.10
23	E1500-4	29.4	0	40.1	48.89	1.22	42.59	1.06
24	E1500-5	50.4	0	37	36.66	0.99	35.72	0.97
25	E1500-6	0	8.4	35.2	36.97	1.05	34.78	0.99
26	E1500-7	0	16.8	27.8	30.82	1.11	28.54	1.03
27	E1500-7	0	29.4	23.4	24.82	1.06	22.93	0.98
28	E1500-7	0	50.4	18	18.72	1.04	17.44	0.97
mean value						1.06		1.00
C.O.V						7.6		6.8

**Tab. 3.** Characteristics of the non-corroded structural elements

ID	Cross-section [mm×mm×mm]	Length [mm]	Relative Slenderness	$b/t$
RF-1	40×40×4	510	0.7	10
RF-2	40×40×4	650	0.9	10
RF-3	40×40×4	840	1.15	10
RF-4	40×40×4	95	1.3	10
RF-5	40×40×4	1100	1.5	10
RF-6	60×60×8	750	0.7	7.5
RF-7	60×60×8	1250	1.15	7.5
RF-8	60×60×8	1640	1.5	7.5
RF-9	100×100×12	1280	0.7	8.3
RF-10	100×100×12	2100	1.15	8.3
RF-11	100×100×12	2760	1.5	8.3

**Tab. 4.** Corrosion patterns and parameters applied in the numerical study

Pattern	$T_{red}$ [%]	$Ext$ [%]	Corrosion position ( $p_c$ )
 "A" pattern	20	20	0.20, 0.47, 0.73, 1.00
	30	30	0.30, 0.53, 0.77, 1.00
	40	40	0.40, 0.70, 1.00
	50	50	0.50, 0.75, 1.00
	60	60	0.50, 0.75, 1.00
 "B" pattern	70	70	0.70, 1.00
	80	80	0.70, 1.00
	100	100	1.00
	100	100	1.00

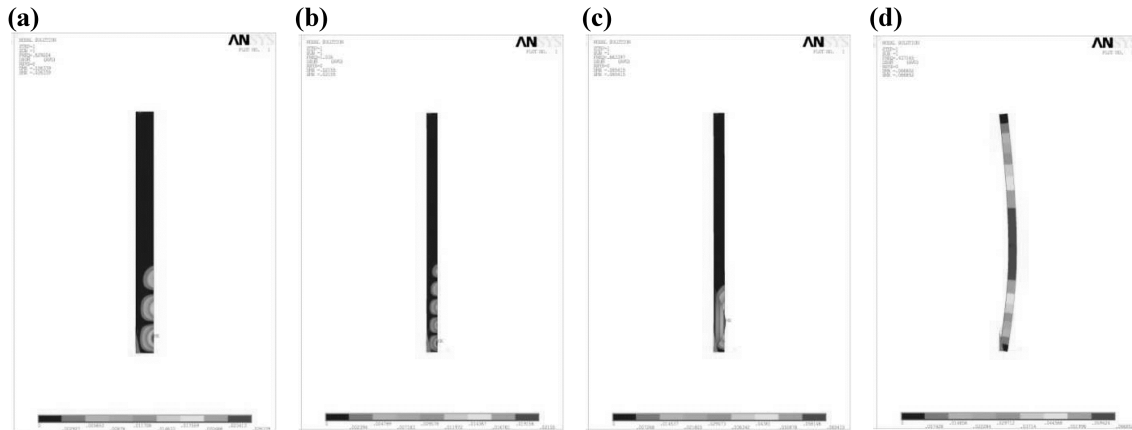


**Fig. 4.** Illustration of buckling modes: (a) local plate buckling  $\bar{\lambda} = 0.7$ ; (b) local plate buckling  $\bar{\lambda} = 1.5$ ; (c) torsional buckling; (d) flexural buckling

towards the damaged region. If the corrosion is unsymmetrical within the cross-section, the axis of the buckling is rotated from the axis of the non-corroded case. In the case of corrosion pattern "A" local buckling occurs. When the corrosion is not close to the support a global flexural buckling mode is perceptible after the occurrence of the yield mechanism. In the case of pattern "B" the typical behaviour is torsional buckling; similarly to the local buckling cases, global flexural buckling is observed after the ultimate load. Figure 5 presents the results of three elements with pattern "A" corrosion and in Fig. 6 the behaviour modes of pattern "B" are presented. In the cases of local buckling behaviour one wave is dominant (as shown in Fig. 4(a)), if the corrosion is close to the support and the number of buckling wave is less than or equal three in buckling mode.

**Tab. 5.** Minimum "necessary" and "sufficient"  $b/t$  ratios

Pattern	Condition	Relative slenderness ( $\bar{\lambda}$ )		
		0.7	1.15	1.5
"A"	necessary	2	25	33.3
	sufficient	18.7	27.8	37.5
"B"	necessary	13.9	18.7	25
	sufficient	18.7	25	33.3

As in the bifurcation stability analysis the "necessary" and "sufficient" values of  $b/t$  ratio are determined to predict the behaviour mode. On the basis of the GMNI results it is concluded

that the same values are valid as presented in Table 5.

The typical load-displacement curves are presented in Fig. 7. Sudden decreasing can be observed on the curves after the ultimate load is reached in the cases of local and torsional buckling. The displacements of the middle point of the corroded part are plotted on the load-horizontal displacement curves.

### 6.2 Imperfection sensitivity

In the previous studies the applied magnitude of the imperfection is  $L/200$  for all the examined elements. This is extended to the range of  $L/1200 - L/200$  in order to investigate the sensitivity of the ultimate behaviour. It is concluded that the behaviour does not change if the failure mode is local or torsional buckling. In the case of global buckling if the relative slenderness is 0.7 the ultimate failure mode can be changed to local buckling; after an initial global buckling the corroded area yields and local buckling occurs. In Fig. 8 the load-vertical displacement curves and the displacements of the middle point are shown (the middle point is located in the corner edge of the middle cross-section of the corroded area). The coordinate axes are the displacements in direction of  $y$  and  $z$  on the right curves of the figure. The effect of the increasing magnitude of imperfection can be followed on the load-displacement curves: after reaching the ultimate load the descending branch decreases rapidly in the case of global buckling and the middle point changes its location. In Fig. 8 results of four ranges of the applied imperfections are presented.

**Tab. 6.** Buckling modes: 1 – global buckling about weak axis, 2 – local plate buckling, 3 – torsional buckling

Part 1							Part 2			Part 3		
$\bar{\lambda} = 0.7$							$\bar{\lambda} = 1.15 \quad b/t = 25$			$\bar{\lambda} = 1.5 \quad b/t = 25$		
Pattern "B"							Pattern "A"			Pattern "B"		
<i>Ext</i>	<i>p<sub>c</sub></i>	<i>b/t</i>					<i>T<sub>red</sub></i>			<i>T<sub>red</sub></i>		
		13.2	13.9	14.3	14.6	15	60	70	66.7	60	70	66.7
20	0,20	3	3	3	3	3	2	2	2	3	3	3
20	0,47	1	1	1	1	1	1	2	2	3	3	3
20	0,73	1	1	1	1	1	1	2	1	1	1	1
20	1,00	1	1	1	1	1	1	1	1	1	1	1
30	0,30	3	3	3	3	3	2	2	2	3	3	3
30	0,53	1	1	1	3	3	1	2	1	3	3	3
30	0,77	1	1	1	1	3	1	1	1	1	1	1
30	1,00	1	1	1	1	1	1	1	1	1	1	1
40	0,40	3	3	3	3	3	1	2	2	3	3	3
40	0,70	1	1	1	3	3	1	1	1	1	1	1
40	1,00	1	1	1	1	3	1	1	1	1	1	1
50	0,50	1	3	3	3	3	1	2	1	1	1	1
50	0,75	1	1	3	3	3	1	1	1	1	1	1
50	1,00	1	1	1	3	3	1	1	1	1	1	1
70	0,70	1	3	3	3	3	1	1	1	1	1	1
70	1,00	1	1	3	3	3	1	1	1	1	1	1
100	1,00	3	3	3	3	3	1	1	1	1	1	1

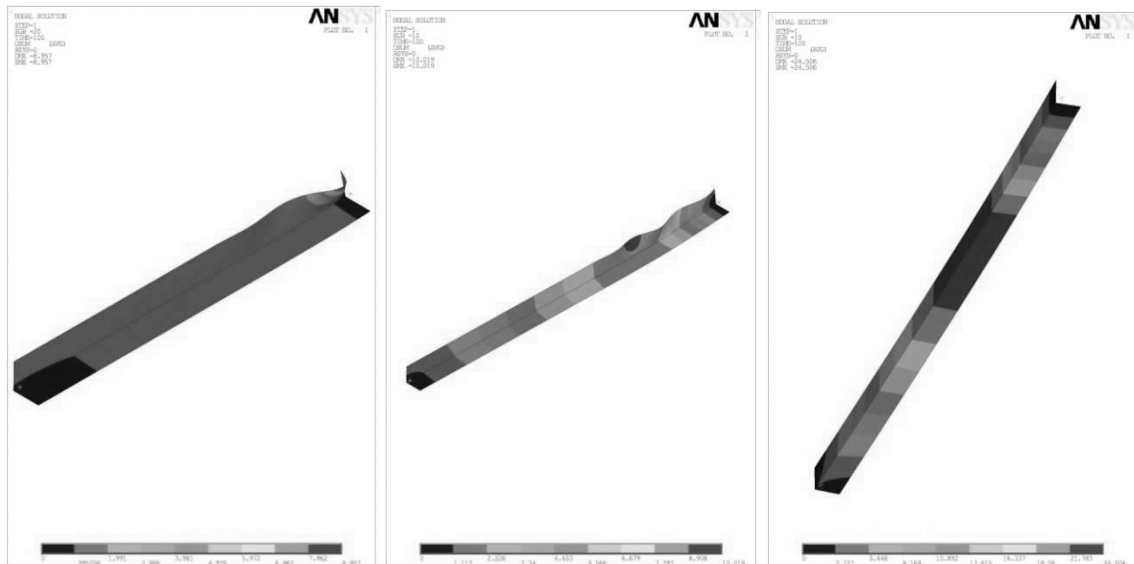


**Fig. 5.** Behaviour modes – corrosion pattern "A"

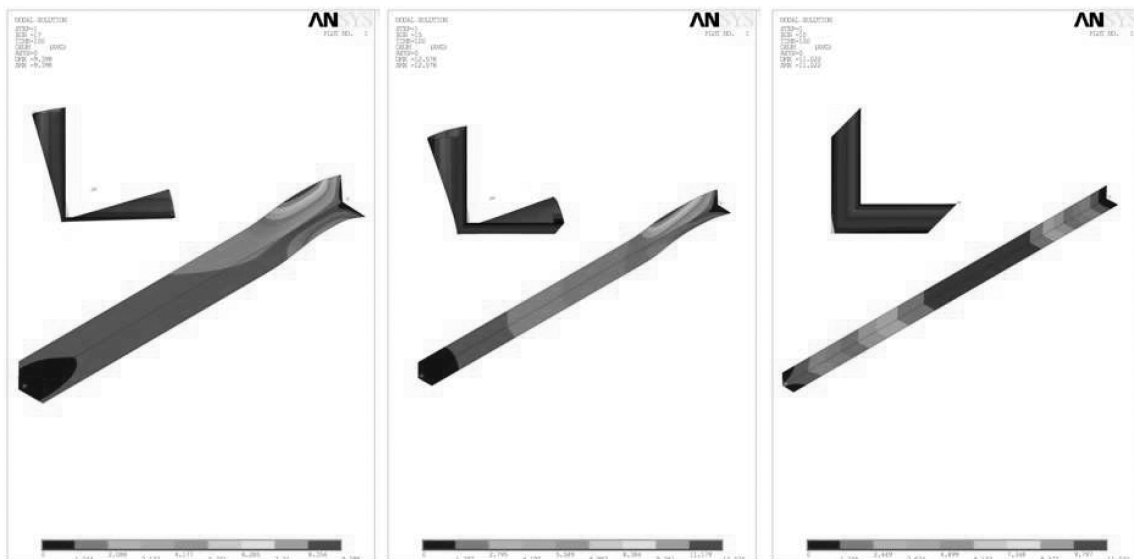


**Fig. 6.** Behaviour modes – corrosion pattern "B"



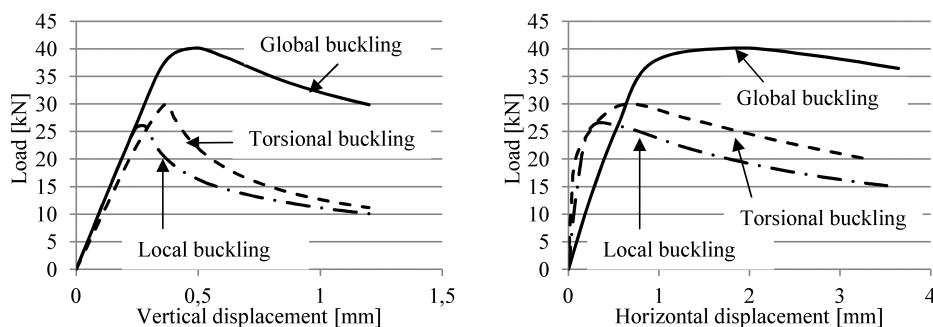


Fig. 7. Typical load-displacement curves

In the case of global buckling the cross-section position is moving from 1 to 2, and in the case of local buckling from 1 to 3 in Fig. 8(b). Changing in the behaviour is observed for the magnitude of appr.  $L/800$  geometric imperfection, in the case of pattern “A”. The reduction of the geometrical imperfection’s magnitude causes increase in resistance.

## 7 Resistances

### 7.1 Observed tendencies

The trivial conclusion of the numerical study is that the corrosion causes decrease in the resistance. In this chapter the decreasing tendency of the resistances is analysed in the function of the corrosion parameters. In the following figures the vertical axis is the ratio of the corroded and the non-corroded elements’ resistances. In Fig. 9 the results of the RF-1 elements are shown; the resistances of the two patterns are plotted separately, the local/torsional and global behaviour modes of the elements are signed. The tendency is different in the cases of the two patterns. By the increasing of the  $b/t$  ratio non-linear decrease in the case of pattern “A” and exponential decrease in the case of pattern “B” are observed. For pattern “A” the elements with local buckling are clearly separated, but it is not unequivocal for pattern “B”. Large standard deviation can be observed in the results for the same  $b/t$  ratio; the difference can be more than 20% in the resistance.

The “necessary” and the “sufficient”  $b/t$  ratios can be followed in Figs. 10–11(a), where the results of the elements with different relative slenderness values are plotted. The sudden decrease in the resistance means that the behaviour is changing from global to local buckling. The number of these cases is decreasing as the relative slenderness is increasing.

The effect of the increasing corrosion extension is different on the resistance of the analysed elements. In the case of pattern “A” (for both global or local behaviours) the increasing extension causes decrease in resistance. While by pattern “B” the increasing extension causes decrease in resistance if the behaviour is global buckling and increase if torsional buckling. Figure 11(b) presents the results of four different elements with various  $T_{red}$  values in the function of the extension of corrosion. The effect of the position of the corrosion on the resistances is presented in Fig. 12. The curves show the results of the elements

for two different  $b/t$  ratios and five relative slenderness values, where the extension is the same in all cases, just the corrosion position is changed. The tendencies are different, non-linear increasing or decreasing in terms of the relative slenderness. The “necessary”  $b/t$  condition of the behaviour mode can be followed e.g. in Fig. 12(a): in the case of relative slenderness 1,15 and if the corrosion is close to the support ( $p_c = 0.2$ ) the decrease is greater than in the case when the corrosion is in the mid-length ( $p_c = 1.0$ ).

In general it can be observed that the change in the corrosion position parameter causes non-linear decrease in resistances as shown in Fig. 12. If the thickness reduction and extension of corrosion are constant parameters, the change of corrosion position causes modification in the behaviour mode and in the tendencies of the resistances. The different corrosion position causes a maximal 17% difference in resistance.

### 7.2 Prediction of the resistance reduction

The joint influence of different corrosion parameters on the behaviour and on the resistance is various, as it is shown in Figs. 9–12. Getting closed formula for the reduction of the resistance is difficult if all of the corrosion and cross-section characteristics are considered. It is essential to consider the changes of the behaviour modes if such a formulation is derived. In Fig. 13 part of the results are plotted in the function of the thickness reduction and the cross-section reduction. The solid straight line marks the tendency, where the resistance reduction is the same as the thickness reduction (Fig. 13(a)) or as the cross-section reduction (Fig. 13(b)). This estimation is not quite accurate, especially in terms of  $C_{red}$ . In the case of  $T_{red}$  the estimation differs from the results about 40% on the safety side or 20% on the opposite side. The values under the estimation line mostly belongs to local behaviour modes.

In Fig. 14(a) the results belonging to elements having pattern “A” and the solid line marks the lowest resistance values of all (both of pattern “A” and “B”) of the analysed RF-1 elements in the function of the thickness reduction. If the estimation is determined by this tendency, the difference between the calculated and the estimated values can be significant. In Fig. 14(b) the curves are determined by the same process as in Fig. 14(a), where the solid lines for all of the investigated elements RF-1–

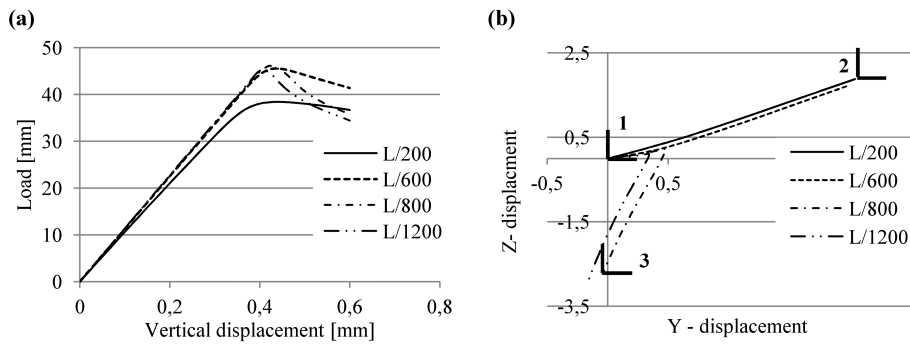


Fig. 8. Effect of the initial imperfection: (a) load-vertical displacement curves; (b) displacements of the middle cross-section

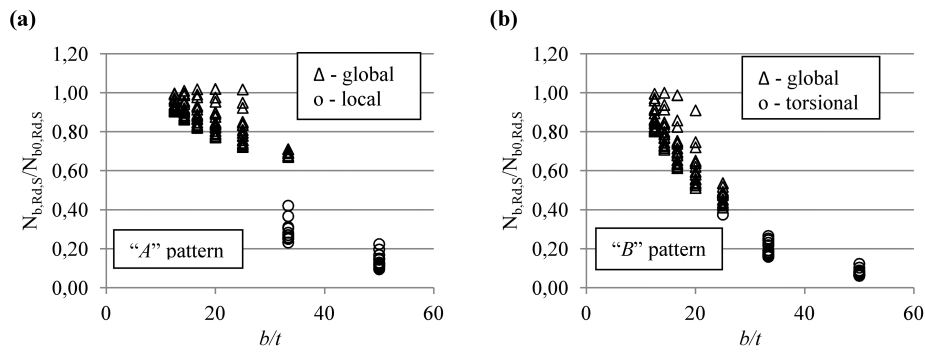


Fig. 9. Resistances of RF-1 elements in the function of the  $b/t$  parameter: (a) pattern "A"; (b) pattern "B"

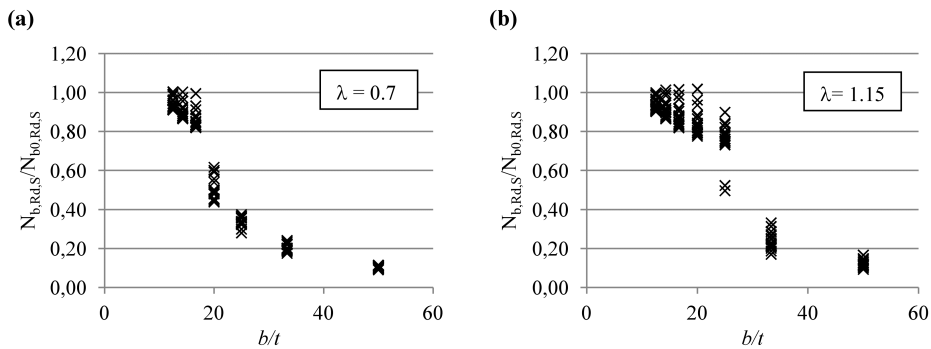


Fig. 10. Resistances of RF-1, RF-3 elements (pattern "A") in the function of the  $b/t$  parameter: (a) RF-1; (b) RF-3

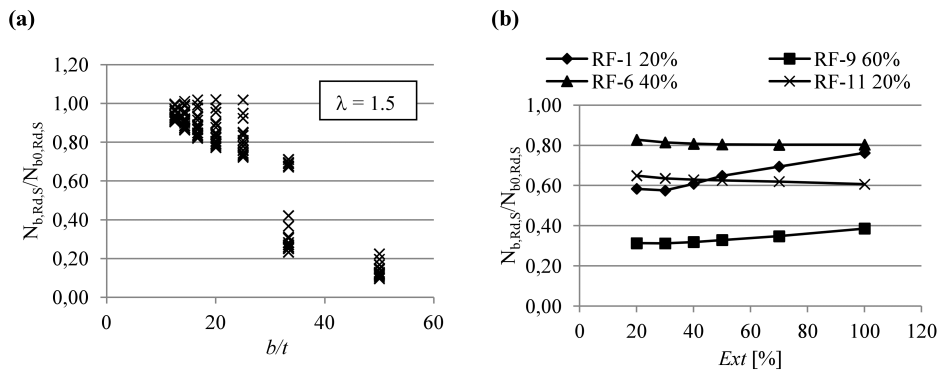


Fig. 11. Resistances: (a) RF-5 elements (pattern "A") in the function of the  $b/t$  parameter, and (b) the effect of extension of corrosion on the resistance de-

crease of pattern "B" elements

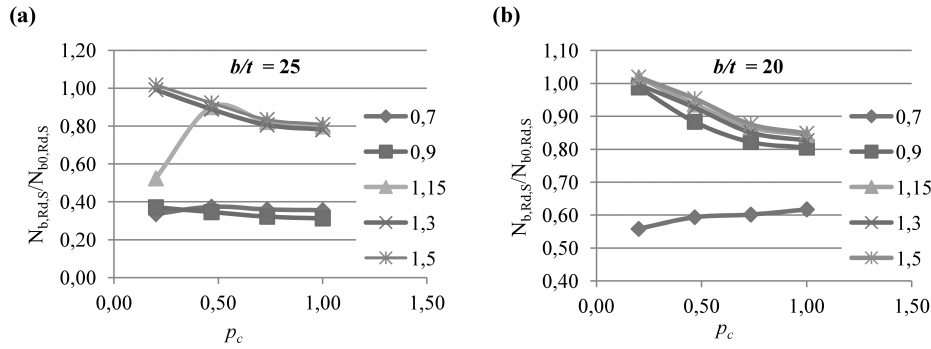


Fig. 12. Resistances of RF-1-5 elements ( $Ext = 20\%$ ) in the function of the  $p_c$  parameter: (a)  $b/t = 25$ ; (b)  $b/t = 20$

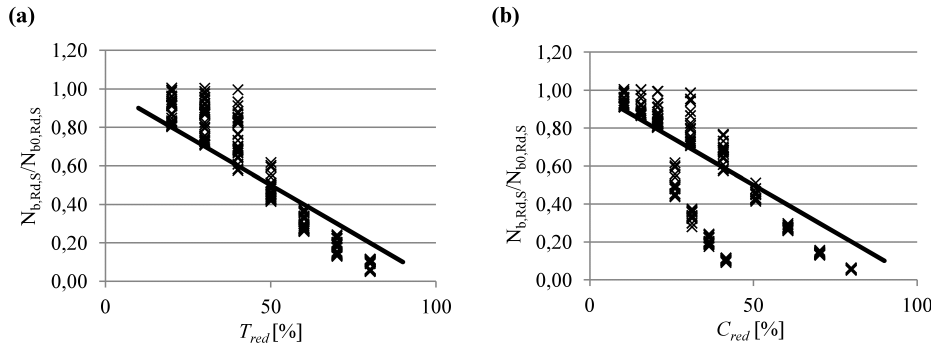


Fig. 13. Resistances of RF-1 elements in the function of the corrosion parameters: (a)  $T_{red}$ ; (b)  $C_{red}$

11 are shown. The tendency is different by the different elements, therefore simplified formula cannot be determined.

Regarding the worst cases, a conservative estimation can be done in terms of the ultimate behaviour. Two corrosion parameters, as the position of corrosion and the extension of corrosion are left out of the estimation. For global buckling behaviour of either pattern “A” or “B” elements, the resistance decrease is approximately equal to the cross-section reduction factor ( $N_{b,Rd,S}/N_{b0,Rd,S} \sim 0.01C_{red}$ ). In the cases of local or torsional buckling, the tendencies are different from global case and depend on the relative slenderness. Figure 15(a) presents the estimation in the cases of pattern “A” and  $\bar{\lambda} = 0.7$ , while in Fig. 15(b) the results of pattern “B” and  $\bar{\lambda} = 0.7$  are shown. The estimation is linear in all cases.

Table 7 contains the equation of the linear approximation of the local and the torsional buckling cases, the dimension of  $C_{red}$  is percentage [%] in the equations.

Tab. 7. Equations of the conservative estimation

	$N_{b,Rd,S}/N_{b0,Rd,S}$	
	Pattern “A”	Pattern “B”
$\bar{\lambda} = 0.7$	$0.995 - 0.023C_{red}$	$1.098 - 0.013C_{red}$
$\bar{\lambda} = 1.15$	$0.73 - 0.016C_{red}$	$1.53 - 0.018C_{red}$
$\bar{\lambda} = 1.5$	$1 - 0.0225C_{red}$	$0.79 - 0.009C_{red}$

If the behaviour mode is global buckling a more accurate approximation formula can be determined, what can be calculated from the thickness reduction ( $T_{red}$ ), the ratio of a modified length ( $L_{mod}$ ) and the total length ( $L$ ), as it is shown in Fig. 16. Part of the results is shown in Fig. 17 in the function of  $L_{mod}/L$ .

The effect of the various extension and corrosion position can be considered by this parameter.

Figure 17(a) presents the results for various  $T_{red}$  and the solid line marks the approximation. The results can be illustrated by a surface in Fig. 17(b), calculated by Eq. (1), in the function of two parameters.

$$N_{b,Rd,S}/N_{b0,Rd,S} = a + b \cdot T_{red} + c \cdot T_{red} \cdot (L_{mod}/L) + d \cdot T_{red} \cdot (L_{mod}/L)^2 \quad (1)$$

The applied  $a$ ,  $b$ ,  $c$  and  $d$  constants are dependent on the relative slenderness.

On the basis of previous experimental and numerical studies the reduction factor was determined for the design buckling resistance of corroded members [18]. Note that the reduction factor is valid only for RF-3 elements of less than 50% cross-section reduction. If the relative slenderness and the initial cross-section change, that estimation is not acceptable, and the above proposals can be used.

## 8 Summary and conclusions

In the current study comprehensive analyses on different corroded angle elements are carried out. The joint influence of the corrosion and cross-section parameters on the behaviour and resistance are investigated. In the numerical study the following parameters are considered: position of corrosion ( $p_c$ ); extension of corrosion ( $Ext$ ); thickness reduction ( $T_{red}$ );  $b/t$  ratio and relative slenderness. In the study two different corrosion patterns are applied, which are typical corrosion appearance in civil engineering practice. The results of the analyses are evaluated in terms of the parameters. On the basis of the results the following

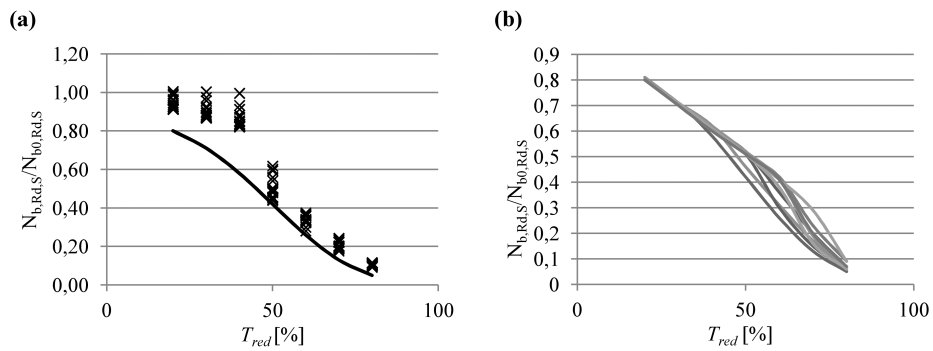


Fig. 14. Approximation and tendencies of resistance reduction for pattern "A": (a) RF-1 element; (b) all of the elements

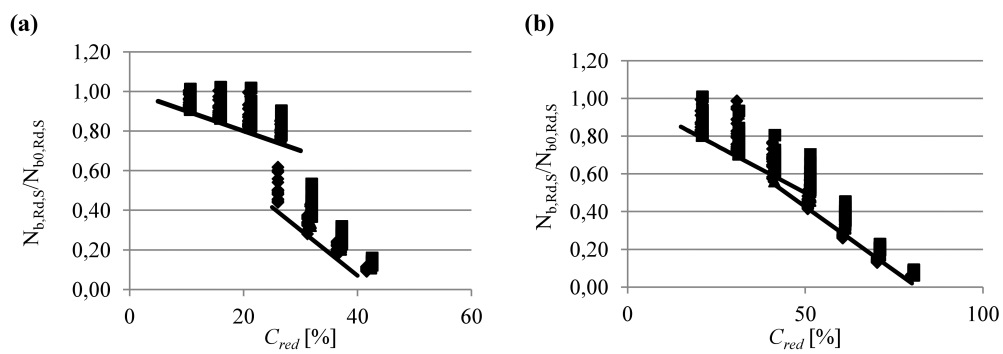


Fig. 15. Conservative estimation: (a) pattern "A" and  $\bar{\lambda} = 0.7$ ; (b) pattern "B" and  $\bar{\lambda} = 0.7$



Fig. 16. Definition of the modified length parameter

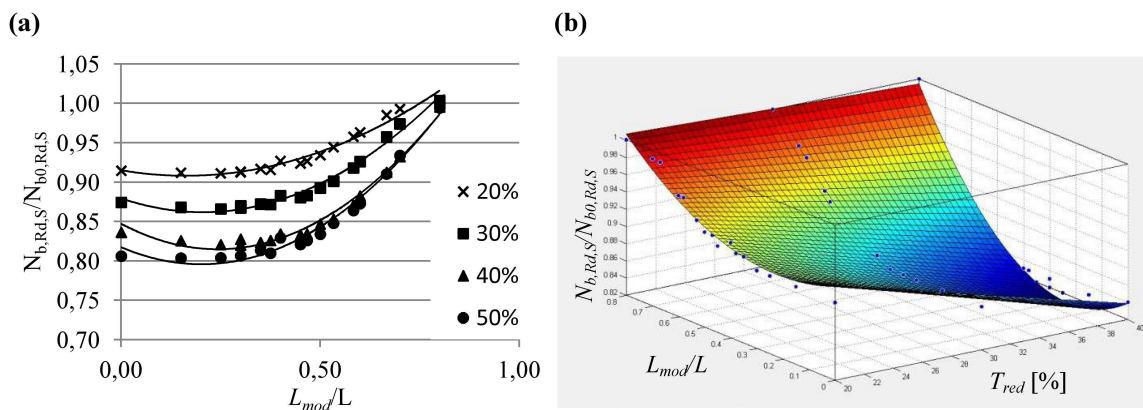


Fig. 17. Resistance reduction results in the function of the modified length parameter: (a) RF-1 elements; (b) the resistance surface

conclusions can be done:

- A parametric finite numerical model is developed; which can model various corrosion damages. The finite element model is calibrated and verified by test results.
- Geometrical non-linear buckling analyses (GNB) are carried out on the corroded elements. The typical buckling modes are determined (local plate buckling, torsional buckling and global flexural buckling). The necessary and sufficient conditions are assessed to determine the buckling behaviour in terms of the corrosion patterns and the relative slenderness.
- Geometrically and material non-linear analyses (GMNI) are carried out using the first buckling mode as initial geometric imperfection. The ultimate behaviour modes are determined, characterised and classified. It is observed that in some cases besides local or torsional buckling, global flexural buckling occurs after the yield mechanism is developed. The effect of the magnitude of the initial geometric imperfection on the behaviour mode is analysed.
- Tendencies of the resistance reduction are determined in the function of the different parameters for the two corrosion patterns. The joint effect of the parameters (extension and position of corrosion,  $b/t$  ratio, thickness reduction, corrosion pattern and relative slenderness) is determined: closed formula is developed to predict the resistance reduction by non-linear regression analysis.

### Acknowledgement

The research has been supported in the framework of the project “Talent care and cultivation in the scientific workshops of BME” project by the grant *TÁMOP – 4.2.2.B-10/1–2010-0009*.

This work is connected to the scientific program of the “Development of quality-oriented and harmonized R+D+I strategy and functional model at BME” project supported by the grant *TÁMOP-4.2.1/B-09/1/KMR-2010-0002*.

### References

- 1 *EN 1993-1-1: Design of steel structures. Part 1-1: General rules and rules for buildings*, 2005.
- 2 **Beaulieu L, Legeron F, Langlois S**, *Compression strength of corroded steel angle members*, Journal of Constructional Steel Research, **66**(11), (2010), 1366–1373, DOI 10.1016/j.jcsr.2010.05.006.
- 3 **Rehgozar R**, *Remaining capacity assessment of corrosion damaged beams using minimum curves*, Journal of Constructional Steel Research, **65**(2), (2009), 299–307, DOI 10.1016/j.jcsr.2008.02.004.
- 4 **Paik J, Lee J, Jo Ko M**, *Ultimate shear strength of plate members with pit corrosion wastage*, Thin-Walled Structures, **42**(8), (2004), 1161–1176, DOI 10.1016/j.tws.2004.03.024.
- 5 **Paik J, Lee J, Jo Ko M**, *Ultimate compressive strength of plate elements with pit corrosion wastage*, Journal of Engineering for the Marine Environment, **217**(4), (2003), 185–200, DOI 10.1177/147509020321700402.
- 6 **Jiang X, Soares C**, *A closed form formula to predict the ultimate capacity of pitted mild plate under biaxial compression*, Thin-Walled Structures, **59**, (2012), 27–34, DOI 10.1016/j.tws.2012.04.007.
- 7 **Khedmati M, Roshanali M, Nouri Z**, *Strength of steel plates with both-sides randomly distributed with corrosion wastage under uniaxial compression*, Thin-Walled Structures, **49**(2), (2011), 325–342, DOI 10.1016/j.tws.2010.10.002.
- 8 **Sadovsky Z, Drdacky M**, *Buckling of plate strip subjected to localised corrosion – a stochastic model*, Thin-Walled Structures, **39**(3), (2001), 247–259, DOI 10.1016/S0263-8231(00)00060-4.
- 9 **Nakai T, Matsushita H, Yamamoto N, Arai H**, *Effect of pitting corrosion on local strength of hold frames of bulk carrier (1st report)*, Marine Structures, **17**(5), (2004), 403–432, DOI 10.1016/j.marstruc.2004.10.001.
- 10 **Nakai T, Matsushita H, Yamamoto N, Arai H**, *Effect of pitting corrosion on local strength of hold frames of bulk carrier (2nd report) - Later-distortional buckling and local face buckling*, Marine Structures, **17**(8), (2004), 612–641, DOI 10.1016/j.marstruc.2005.03.001.
- 11 **Liu Y, Hui L**, *Experimental study of beam-column behaviour of steel single angles*, Journal of Constructional Steel Research, **64**(5), (2008), 505–514, DOI 10.1016/j.jcsr.2007.11.002.
- 12 **Liu Y, Hui L**, *Finite element study of steel single angle beam-columns*, Engineering Structures, **32**(8), (2010), 2087–2095, DOI 10.1016/j.engstruct.2010.03.009.
- 13 **Liu Y, Chantel S**, *Experimental study of steel single unequal-leg angles under eccentric compression*, Journal of Constructional Steel Research, **67**(6), (2011), 919–928, DOI 10.1016/j.jcsr.2011.02.005.
- 14 **Oszvald K, Dunai L**, *Effect of corrosion on the buckling of steel angle members - experimental study*, Periodica Polytechnica - Civil Engineering, **56**(2), (2012), 175–183, DOI 10.3311/pp.ci.2012-2.04.
- 15 *ANSYS Release 11.0 Documentation*, Ansys Inc., 2007.
- 16 **Kövesdi B, Kuhlmann U, Dunai L**, *Combined shear and patch loading of girders with corrugated webs*, Periodica Polytechnica - Civil Engineering, **54**(2), (2010), 79–88, DOI 10.3311/pp.ci.2010-2.02.
- 17 **Oszvald K, Dunai L**, *Effect of corrosion on the buckling of steel angle elements*, 8th International PhD Symposium in Civil Engineering, (Lyngby, Denmark, 2010-06), In: **Fisher G, Geiker M, Hededal O, Ottosen L, Stang H** (eds.), Proceedings 8th International PhD Symposium in Civil Engineering, Department of Civil Engineering, Technical University of Denmark, 2010, pp. 549–554.
- 18 **Oszvald K, Dunai L**, *Design buckling resistance of corroded members, determining the reduction factor for angle section elements*, 6th European Conference on Steel and Composite Structures, (Budapest, Hungary, 2011-08), In: **Dunai L, Iványi M, Jármai K, Kovács N, Vigh L** (eds.), Proceedings of EUROSTEEL 2011, ECCS European Convention for Constructional Steelwork, 2011, pp. 627–632.